ResearchGate

See discussions, stats, and author profiles for this publication at: https://www.researchgate.net/publication/270427259

Inclinodeformeter pressure measurements in creeping landslides: Analytical solutions and field applications

Article *in* Géotechnique · May 2014

DOI: 10.1680/geot.13.P.185

CITATIONS
5

READS
280

2 authors:



Markus V. Schwager
Swiss Federal Office of Energy (SFOE)
11 PUBLICATIONS **20** CITATIONS

SEE PROFILE



Alexander M. Puzrin
ETH Zurich
220 PUBLICATIONS **2,777** CITATIONS

SEE PROFILE

Some of the authors of this publication are also working on these related projects:

Geotechnical and Structural Health Monitoring View project

Hyperplasticity View project

All content following this page was uploaded by Markus V. Schwager on 12 April 2016.

The user has requested enhancement of the downloaded file.

Schwager, M. V. & Puzrin, A. M. (2014). *Géotechnique* **64**, No. 6, 447–462 [http://dx.doi.org/10.1680/geot.13.P.185]

Inclinodeformeter pressure measurements in creeping landslides: analytical solutions and field applications

M. V. SCHWAGER* and A. M. PUZRIN*

The paper derives analytical solutions for deformation of viscoelastic pipe in elastic soil under far-field principal stress increments. These solutions are validated in laboratory tests and numerical analysis and provide the basis for back-calculation of earth pressure increments from measured changes in shape of an inclinometer pipe cross-section using inclinodeformeter (IDM) technology. The procedure has been applied to back-calculating earth pressure changes and soil stiffness in three creeping landslides in Switzerland, which are similar in size but have a range of different boundary conditions and displacement rate fields. In these applications, pressure increments of less than 1 kPa could be reliably back-calculated allowing for identification of compression and extension zones, as well as yielding and failure of soil in the landslides under study, confirming the previously developed models of the landslide mechanisms and suggesting that IDM pressure measurements could serve as a reliable tool for analysis and monitoring of creeping landslides.

KEYWORDS: case history; creep; earth pressure; field instrumentation; landslides; monitoring

INTRODUCTION

Understanding the earth pressure changes in a sliding layer of a creeping landslide is essential for analysis and stabilisation of such landslides. In particular, the rate of change of the lateral earth pressure has been found to be a critical parameter for the validation of models for constrained creeping landslides (Puzrin & Schmid, 2011, 2012; Puzrin *et al.*, 2012).

The inclinodeformeter (IDM) is a novel device for back-calculation of the changes of earth pressure in the sliding layer of creeping landslides. Its concept has been presented by Schwager *et al.* (2010). IDM measures the change in dimensions of an inclinometer pipe and uses the measured deformations to back-calculate the change in pressure by solving the corresponding boundary value problem.

IDM makes use of the widespread inclinometer technology. In addition to the regular displacement profile, the IDM probe also provides a continuous profile of lateral earth pressures, using the same inclinometer pipe and requiring no further installation on the site.

In this paper a simplified procedure is introduced for back-calculating the earth pressure changes. This procedure required the derivation of analytical solutions for deformation of viscoelastic pipes in elastic space under corresponding boundary conditions and calibration of these solutions against results of laboratory tests and numerical analysis. The procedure has then been applied to measuring earth pressure changes in three creeping landslides in Switzerland. These landslides are similar in size, but have different boundary conditions and displacement rate fields, as listed below.

(*a*) The St Moritz-Brattas landslide is slowing downhill towards a rock outcrop at the bottom.
(*b*) The Braunwald landslide is accelerating downhill towards a vertical rock wall falling into a valley.
(*c*) The Ganter landslide is moving uniformly downhill towards a river bed.

Pressure measurements taken by IDM allow the identification of compression and extension zones in the sliding body and provide unique quantitative data for understanding and mechanical analysis of these creeping landslides.

Manuscript received 5 November 2013; revised manuscript accepted 4 April 2014. Published online ahead of print 6 June 2014.
Discussion on this paper closes on 1 November 2014, for further details see p. ii.
* Institute for Geotechnical Engineering, ETH Zurich, Zurich, Switzerland.

MEASURING DEFORMATIONS OF THE INCLINOMETER PIPE

In order to measure inclinometer pipe deformations, the IDM probe is lowered down the pipe guided by three wheels along a pair of grooves or channels (Schwager *et al.*, 2010). The upper and lower wheels roll in the same channel (Figs 1(a) and 1(b)). These wheels are fixed to the probe. The middle wheel is connected by way of a lever with two springs and is pressed against the opposite channel. A change in the pipe diameter leads to a change of the position of the middle wheel with respect to the probe. There are two tilt sensors to measure the inner diameter of the pipe: one sensor is located on the top of the probe and detects the inclination of the probe α_P; another tilt sensor is located on the lever of the middle wheel and detects the inclination of the lever α_L. The inner diameter D is a function of the relative inclination $(\alpha_L - \alpha_P)$.

Diameter D_A (Fig. 1(c)) between the channels in direction A, where the larger displacements are expected, is measured first; direction B is perpendicular to A (Fig. 1(c)). In addition, continuous measurements are taken of the inclination of the probe in both directions A and B, of the temperature and of the water pressure in the pipe, at a frequency of 40 readings per 1 cm of depth.

After completing measurements of diameter D_A, the probe is rotated by 90° and lowered down again, guided along the second pair of channels, so that the diameter D_B can be measured along the pipe length. Because the tilt sensors (α_L, α_P) are not independent of the inclination of the pipe out of the plane, both diameter readings are corrected for the influence of this inclination (Schwager *et al.*, 2010). A correction function calibrated in laboratory tests is applied.

Next, the pipe ovalisation value Ω is calculated, defined

Downloaded by [ETH Zurich] on [12/04/16]. Copyright © ICE Publishing, all rights reserved.

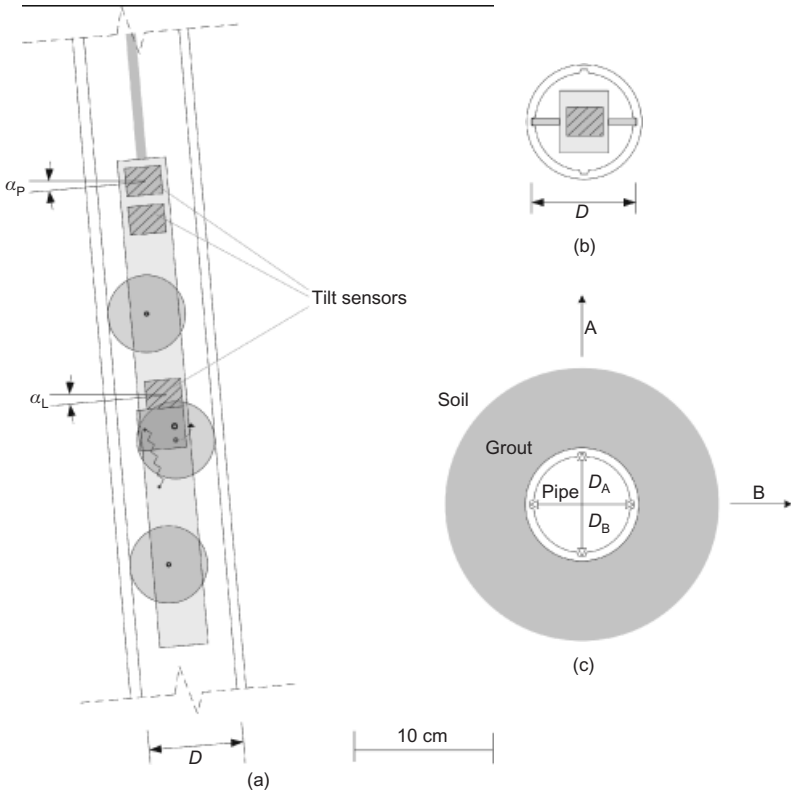


Fig. 1. The IDM diameter measurements: (a) side view of the IDM probe in the inclinometer pipe; (b) top view of the IDM probe in the inclinometer pipe; (c) measured diameters in a horizontal cross-section of the installed inclinometer pipe

as the difference of the perpendicular diameters normalised by the nominal outer radius of the inclinometer pipe R.

$$\Omega = \frac{D_B - D_A}{R} \tag{1}$$

Unlike individual diameter measurements, the difference between the measured diameters does not appear to be sensitive to the temperature of the probe, long-term instability of the probe sensors, wear of the wheels, or to the influence of actual measurement conditions causing a uniform radial expansion or contraction of the pipe (such as temperature of the pipe, water pressures inside and outside the pipe). Deformation changes of the pipe are always measured (and the corresponding pressure changes are back-calculated) relative to the first measurement in time, the so-called zero-measurement. Further measurements at later points in time are taken after an expected change in lateral earth pressure has taken place. The deformation is described by the change in ovalisation value $\Delta\Omega$ with respect to the zero measurement

$$\Delta\Omega_n = \Omega_n - \Omega_0 = \frac{(D_{B,n} - D_{A,n}) - (D_{B,0} - D_{A,0})}{R} \tag{2}$$

Deformations of the pipe cross-section occur not only due to changes in earth pressures, but also as a result of the inclinometer pipe bending, causing its cross-section to flatten into an oval. The inclinometer pipe is subjected to bending due to displacements of the surrounding soil, which may not be related to earth pressure changes. The measured change in ovalisation value can be corrected for bending, as described by an analytical formula calibrated against numerical simulations (Schwager, 2013). However, if the pipe curvature is reasonably small, as is the case for many applications for IDM, no correction is necessary. Schwager (2013) defined this threshold curvature as $\left|\chi_n^2 - \chi_0^2\right| \leqslant 1{\cdot}7 \times 10^{-10}\text{mm}^{-2}$, where χ_n is the current curvature and χ_0 is the initial curvature. The field measurements presented in this paper have been obtained sufficiently far from the shear surface, so that the bending curvature did not exceed this threshold value. Therefore the cross-section deformation due to bending could be neglected for this study.

While the ovalisation measurements are taken continuously over the thickness of the sliding layer, for back-calculation of the pressure changes a certain level of averaging and discretisation is required to eliminate measurement noise. The inclinometer pipe is made out of 3 m long casing elements. Each casing element is treated as one sensor, with the measurements averaged within the element over the length of 12 times the circumference of the wheels of the probe in order to reduce the influence of their imperfection. This leaves about 44 cm at the edges of the casing element which are neglected to eliminate the effects of the joints between the elements.

ANALYTICAL SOLUTIONS FOR BACK-CALCULATION OF PRESSURES

Boundary value problem: assumptions

The pressure increments casing deformations of a pipe cross-section in soil can be back-calculated from a solution of the corresponding boundary value problem, provided that the stiffness of the pipe, grout and soil are known in this range of pressures. Owing to the overburden, the vertical direction is assumed to be a principal stress direction with constant normal stress. The remaining non-zero components of the incremental stress tensor (i.e. the two principal stress increments $\Delta\sigma_1$ and $\Delta\sigma_2$ in the horizontal plane) are back-calculated by considering the boundary value problem given by a horizontal cross-section under generalised plane stress

Downloaded by [ETH Zurich] on [12/04/16]. Copyright © ICE Publishing, all rights reserved.

conditions (Fig. 2). Within the plane, one principal stress direction of the increment is assumed to coincide with the direction of displacement, which is known from the conventional inclinometer measurements. The creeping landslides under consideration have wide moving fronts. Therefore, far away from the inclinometer pipe no horizontal displacements are assumed to occur in the direction perpendicular to the inclinometer measured displacement. Full slippage is assumed at the interface between the pipe and the soil. Radial deformations through the thickness of the pipe are assumed to be small.

Inclinometer pipes are fixed in the boreholes by grouting the annulus (Fig. 1(c)), with the grout around inclinometer pipes often chosen to mimic the deformation characteristics of the surrounding soil. Influence of the grout stiffness on the back-calculation of stresses is addressed in Schwager (2013). It appears that the back-calculation of stresses is not sensitive to the grout stiffness (Fig. 3), with a ten-fold increase in the grout stiffness causing less than 30% maximum error in the back-calculated stress increments. Therefore, in the solution below it is assumed that the grout has the same stiffness as the sliding mass.

Boundary value problem: solution strategy

The solution for deformations of the viscoelastic pipe embedded in elastic soil under the far-field principal stress increments is derived through the following auxiliary steps.

(*a*) First, deformations of the unsupported cylindrical cavity in elastic soil under far-field principal stress increments will be calculated.

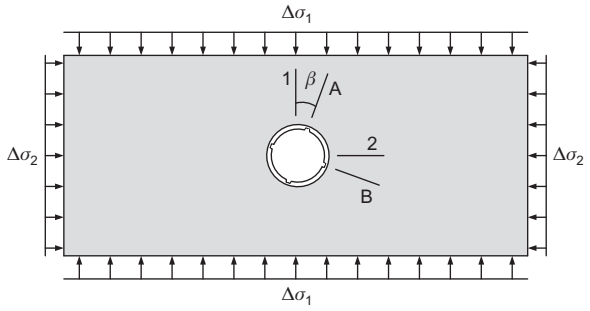


Fig. 2. Schematic layout of the boundary value problem

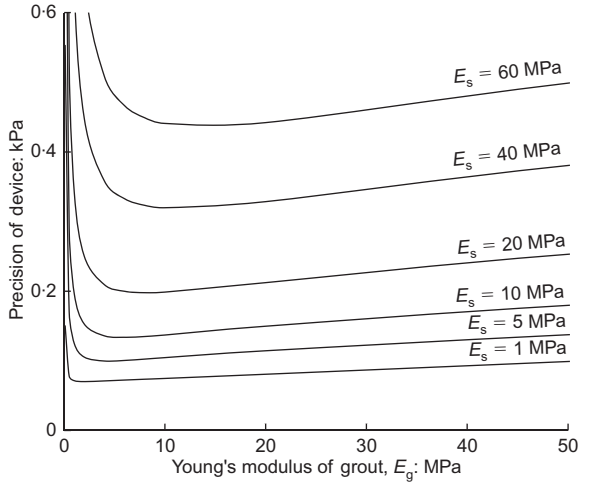


Fig. 3. Pressures causing the lowest detectable ovalisation as a function of the Young's modulus of the grout, calculated for the following assumptions: Young's modulus of the pipe $E_p = 2000$ MPa; Poisson ratio of the pipe $\nu_p = 0.34$; Poisson ratio of the grout $\nu_g = 0{\cdot}2$; Poisson ratio of the soil $\nu_s = 0{\cdot}2$

(*b*) Second, a solution of the same problem, but with loaded cavity and zero far-field principal stress increments is derived.

(*c*) Third, the general solution is derived for the deformations of the viscoelastic pipe subjected to variable radial pressures.

Finally, the pipe deformations caused by far-field changes in lateral earth pressure are obtained by combination of the three solutions derived above (i.e. deformation of the cylindrical cavity due to lateral earth pressure increments $u^{\Delta\sigma_1}$, deformation of the cavity due to pressure at the inclusion u^q and deformation of the pipe due to external pressure u^p).

Indeed, compatibility of the soil and the pipe displacements in the radial direction requires

$$u^{\Delta\sigma_1}(r = R, \theta, t) + u^q(r = R, \theta, t) = u^p(r = R, \theta, t) \qquad (3)$$

which, combined with the equilibrium of pressures at the boundary between the pipe and the cavity, allows for calculation of the deformation of the cross-section of a viscoelastic pipe embedded in elastic soil under the far-field principal stress increments.

Unsupported cylindrical cavity under far-field principal stress increments

In the first auxiliary step, deformations of the unsupported cylindrical cavity under far-field principal stresses are going to be derived (Fig. 4(a)). The principal pressures at infinite distance from the cavity are assumed to be $\Delta\sigma_1$ and $\Delta\sigma_2 = K_0\Delta\sigma_1$ owing to the far-field plane strain condition perpendicular to the landslide front, where $K_0 = \nu_s$. The static boundary conditions are decomposed into a hydrostatic component $\Delta\sigma_1(1 + K_0)/2$ and a deviatoric component $\pm\Delta\sigma_1(1 - K_0)/2$. The uniform contraction of the cavity caused by the hydrostatic component can be neglected because it has to be identical to the uniform contraction of the pipe, which is negligible compared to its ovalisation. For the remaining deviatoric component, solution of the boundary value problem is the well-known Michell solution (e.g. Barber, 2002)

$$u^{\Delta\sigma_1}(r = R, \theta) = -\frac{2R\Delta\sigma_1(1 - K_0)\cos(2\theta)}{E_s} \qquad (4)$$

where E_s is the Young's modulus and ν_s is the Poisson ratio of the soil; R is the radius of the cavity (identical to the outer radius of the pipe) and K_0 is the ratio between the two principal stresses in the plane.

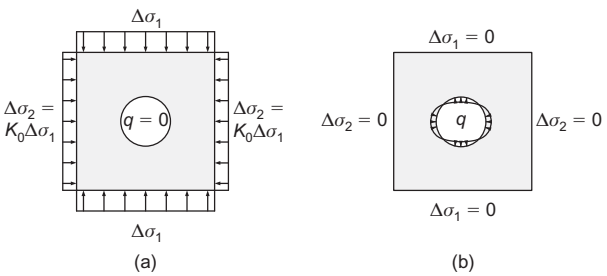


Fig. 4. Schematic layout of the two auxiliary boundary value problems: (a) unsupported cylindrical cavity under far-field principal stress increments; (b) loaded cylindrical cavity with zero far-field principal stress increments

Downloaded by [ETH Zurich] on [12/04/16]. Copyright © ICE Publishing, all rights reserved.

Unsupported cylindrical cavity loaded by a variable radial pressure

The second auxiliary step requires solving the boundary value problem for the cylindrical cavity loaded by the pressure $-q(t)\cos(n\theta)$ at $r = R$, $n = 2, \ldots$ and zero far-field principal stresses (Fig. 4(b)). Solution of this boundary value problem is another well-known Michell solution (e.g. Penzien & Wu, 1998; Barber, 2002):

$$u^q(r = R, \theta) = \frac{Rq(t)\cos(\mathrm{n}\theta)(5 - \nu_\mathrm{s})}{3E_\mathrm{s}} \tag{5}$$

Viscoelastic solution for the pipe under plane stress conditions

In the third auxiliary step, viscoelastic deformations are derived for the pipe subjected to a variable radial pressure. Inclinometer pipes used in this study are made out of polyvinyl chloride (PVC). They show a time-dependent mechanical behaviour, which can be described by the viscoelastic Burgers model (Schwager *et al.*, 2012). An analytical solution for the radial deformation of a pipe without channels is derived below for the case of constant pressure (creep) and constantly increasing pressure (constant rate), relevant for the long-term loading conditions in creeping landslides.

The external pressure $p(\theta, t)$ acting on the pipe is assumed to be the following function of the circumferential coordinate and time

$$p(\theta, t) = -p_n(t)\cos(n\theta) \quad n \geqslant 2 \tag{6}$$

where n is an integer number. The hydrostatic case of $n = 0$ is neglected, because no ovalisation is formed. The case of $n = 1$ is ignored owing to the lack of equilibrium. Static equilibrium of the thin-walled pipe in plane stress conditions is given by (Fig. 5(a))

$$V\mathrm{d}\theta + \mathrm{d}N = 0 \tag{7}$$

$$\mathrm{d}V - N\mathrm{d}\theta + p(\theta, t)R_\mathrm{m}\mathrm{d}\theta = 0 \tag{8}$$

$$\mathrm{d}M - VR_\mathrm{m}\mathrm{d}\theta = 0 \tag{9}$$

where R_m is the mean radius of the pipe, N is the internal normal force, V is the shear force and M is the moment.

Combining equilibrium equations (7)–(9), the following differential equations are obtained for the normal force and the moment

$$\frac{\mathrm{d}^2N}{\mathrm{d}\theta^2} + N = -p_n(t)R_\mathrm{m}\cos(n\theta) \tag{10}$$

$$\frac{\mathrm{d}^2M}{\mathrm{d}\theta^2} + M = p_n(t)R_\mathrm{m}^2\cos(n\theta) \tag{11}$$

Because the symmetry is required to be the same as for the applied pressure, the solutions of the equations (10) and (11) are given by

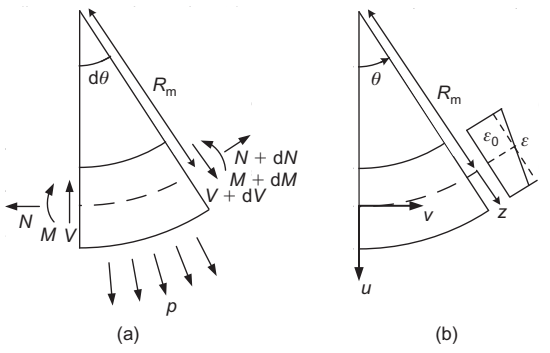


Fig. 5. Notation of (a) internal and external forces, and (b) displacements and strains

$$N(\theta, t) = \frac{1}{n^2 - 1}p_n(t)R_\mathrm{m}\cos(n\theta) \tag{12}$$

$$M(\theta, t) = \frac{-1}{n^2 - 1}p_n(t)R_\mathrm{m}^2\cos(n\theta) \tag{13}$$

According to Bouma (1993), from the compatibility considerations, the strain profile through the thickness of the pipe (Fig. 5(b)) can be described as

$$\varepsilon(z) = \frac{R_\mathrm{m}}{R_\mathrm{m} + z}(\varepsilon_0 + \chi z) \tag{14}$$

where $\varepsilon_0 = \varepsilon(0)$ and $\chi = \varepsilon'(0) + \varepsilon(0)/R_\mathrm{m}$, which are related to the radial displacement u and the tangential displacement v by the kinematic equations

$$\varepsilon_0(\theta, t) = \frac{1}{R_\mathrm{m}}\left(\frac{\partial v}{\partial \theta} + u\right) \tag{15}$$

$$\chi(\theta, t) = \frac{1}{R_\mathrm{m}^2}\left(\frac{\partial v}{\partial \theta} - \frac{\partial^2 u}{\partial \theta^2}\right) \tag{16}$$

The constitutive equation of the pipe material in terms of circumferential stress and strain is given by the Burgers model (Fig. 6)

$$\sigma + p_1\dot{\sigma} + p_2\ddot{\sigma} = q_1\dot{\varepsilon} + q_2\ddot{\varepsilon} \tag{17}$$

where q_1, q_2, p_1 and p_2 are parameters of the Burgers model

$$p_1 = \frac{\eta_0}{E_0} + \frac{\eta_1}{E_1} + \frac{\eta_0}{E_1};\ p_2 = \frac{\eta_0\eta_1}{E_0E_1};\ q_1 = \eta_0;\ q_2 = \frac{\eta_0\eta_1}{E_1} \tag{18}$$

The wall of the ring is considered to be thin. Therefore, neglecting higher order terms (Bouma, 1993) gives the following viscoelastic constitutive equations in terms of forces and moments (Appendix 1)

$$N + p_1\dot{N} + p_2\ddot{N} = q_1\left(A\dot{\varepsilon}_0 - \frac{I}{R_\mathrm{m}}\dot{\chi}\right) + q_2\left(A\ddot{\varepsilon}_0 - \frac{I}{R_\mathrm{m}}\ddot{\chi}\right) \tag{19}$$

$$M + p_1\dot{M} + p_2\ddot{M} = q_1\left(-\frac{I}{R_\mathrm{m}}\dot{\varepsilon}_0 + I\dot{\chi}\right) + q_2\left(-\frac{I}{R_\mathrm{m}}\ddot{\varepsilon}_0 - I\ddot{\chi}\right) \tag{20}$$

where $A = 1 \times h$ is the area and $I = 1 \times h^3/12$ is the moment of inertia of the cross-section.

Equations (12) and (13), equations (15) and (16), and equations (19) and (20) are static, kinematic and constitutive equations, respectively, constituting together with the loading condition (equation (6)) the viscoelastic boundary value problem for a thin pipe under plane stress conditions. This problem will be solved using the elastic–viscoelastic correspondence principle (e.g. Findley *et al.*, 1976).

As the first step, a simpler elastic problem will be solved. Assuming for the pipe material purely elastic constitutive behaviour in terms of circumferential stress and strain

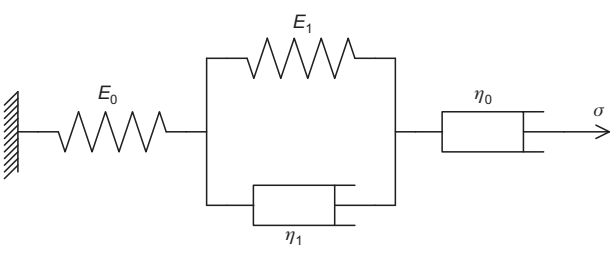


Fig. 6. Linear viscoelastic Burgers model

Downloaded by [ETH Zurich] on [12/04/16]. Copyright © ICE Publishing, all rights reserved.

$\sigma = E\varepsilon$, equations (19) and (20) reduce to the following elastic constitutive equations in terms of forces and moments

$$N = E\left(A\varepsilon_0 - \frac{I}{R_m}\chi\right) \tag{21}$$

$$M = E\left(-\frac{I}{R_m}\varepsilon_0 + I\chi\right) \tag{22}$$

Combining equations (12) and (13), equations (15) and (16), and equations (21) and (22) results in the following differential equation of the elastic boundary value problem

$$u + \frac{\partial^2 u}{\partial\theta^2} = \frac{1}{n^2-1}\frac{R_m^4}{EI}p_n\cos(n\theta) \tag{23}$$

which has the solution

$$u(\theta) = -\frac{1}{(n^2-1)^2}\frac{R_m^4}{EI}p_n\cos(n\theta) \tag{24}$$

In the second step, equations (12) and (13), equations (15) and (16), and equations (19) and (20) of the viscoelastic boundary value problem are transformed into Laplace space

$$\hat{N}(\theta, s) = \frac{1}{n^2-1}\hat{p}_n(s)R_m\cos(n\theta) \tag{25}$$

$$\hat{M}(\theta, s) = \frac{-1}{n^2-1}\hat{p}_n(s)R_m^2\cos(n\theta) \tag{26}$$

$$\hat{\varepsilon}_0(\theta, s) = \frac{1}{R_m}\left(\frac{\partial\hat{v}}{\partial\theta} + \hat{u}\right) \tag{27}$$

$$\hat{\chi}(\theta, s) = \frac{1}{R_m^2}\left(\frac{\partial\hat{v}}{\partial\theta} - \frac{\partial^2\hat{u}}{\partial\theta^2}\right) \tag{28}$$

$$\hat{N} = \frac{q_1 s + q_2 s^2}{1 + p_1 s + p_2 s^2}\left(A\hat{\varepsilon}_0 - \frac{I}{R_m}\hat{\chi}\right) \tag{29}$$

$$\hat{M} = \frac{q_1 s + q_2 s^2}{1 + p_1 s + p_2 s^2}\left(-\frac{I}{R_m}\hat{\varepsilon}_0 + I\hat{\chi}\right) \tag{30}$$

Equations (25)–(30) are equivalent to equations (12) and (13), equations (15) and (16), and equations (21) and (22) of the elastic boundary value problem where the elastic modulus E is replaced by the transformed modulus

$$\hat{E}(s) = \frac{q_1 s + q_2 s^2}{1 + p_1 s + p_2 s^2} \tag{31}$$

Finally, according to the elastic–viscoelastic correspondence principle, the solution is equivalent to the elastic one in equation (24) where true variables are replaced by the corresponding transformed ones

$$\hat{u}(\theta, s) = -\frac{1}{(n^2-1)^2}\frac{R_m^4}{I}\frac{q_1 s + q_2 s^2}{1 + p_1 s + p_2 s^2}\hat{p}_n\cos(n\theta) \tag{32}$$

The inverse Laplace transformation is applied to equation (32) first for the case of a load function of $p_n = \text{const}$ corresponding to the transformed value of

$$\hat{p}_n(s) = \frac{p_n}{s} \tag{33}$$

and then for the case of a load function of $\dot{p}_n = \text{const}$ corresponding to

$$\hat{p}_n(s) = \frac{\dot{p}_n}{s^2} \tag{34}$$

The resulting transformation to the time domain yields the viscoelastic solution

$$u(\theta, t) = -\frac{1}{(n^2-1)^2}\frac{R_m^4}{I}p_n\cos(n\theta) \times \left[\frac{1}{E_0} + \frac{1}{E_1}(1 - e^{-(E_1/\eta_1)t}) + \frac{1}{\eta_0}t\right] \tag{35}$$

for creep conditions with constant pressure p_n, and

$$u(\theta, t) = -\frac{1}{(n^2-1)^2}\frac{R_m^4}{I}\dot{p}_n\cos(n\theta) \times \left[\frac{\eta_1}{E_1^2}(e^{-(E_1/\eta_1)t} - 1) + \frac{1}{2\eta_0}t^2 + \left(\frac{1}{E_0} + \frac{1}{E_1}\right)t\right] \tag{36}$$

for constant stress rate conditions with constant pressure rate $\dot{p}_n$.

Combined solution for the pipe–soil interaction

As is seen from equation (4), the increment of the far-field principal stresses causes radial displacements of the cylindrical cavity proportional to $\cos(n\theta)$, where $n = 2$. These displacements will have to be compatible with the corresponding pipe displacements from equations (35) and (36), that is, the deformation mode of the pipe will also be defined by $\cos(n\theta)$, with $n = 2$. According to equation (6), this is only possible if the pressures acting on the pipe are proportional to $\cos(2\theta)$. According to the Third Law of Newton, the same pressures with the opposite sign will act on the boundary of the cavity. Therefore, in the second auxiliary step the cylindrical cavity will be loaded by the pressure $-q(t)\cos(2\theta)$ at $r = R$ and zero far-field principal stresses, which, following equation (5), also produce the cavity deformation mode proportional to $\cos(2\theta)$, compatible with the corresponding pipe deformation mode.

Thus, the pipe deformations caused by changes in lateral earth pressure are obtained by combination of the derived solutions (i.e. deformation of the cylindrical cavity due to lateral earth pressure increments $u^{\Delta\sigma_1}$, deformation of the cavity due to pressure at the inclusion u^q and deformation of the pipe due to external pressure u^p, both for the deformation mode of $n = 2$), provided the equilibrium of pressures at the boundary between the pipe and the cavity and the compatibility of the soil and the pipe displacements in the radial direction are satisfied

$$u^{\Delta\sigma_1}(r = R, \theta, t) + u^q(r = R, \theta, t) = u^p(r = R, \theta, t) \approx u^p(r = R_m, \theta, t) \tag{37}$$

For formulating the equilibrium condition for the pressures at the boundary between the pipe and cylindrical cavity, the true pressure q on the outside radius R of the pipe has to be related to the pressure boundary condition for the thin-walled pipe solution: the pressure p acting at the radius R_m. For this, the thin-walled solution and the thick-walled solution are required to produce the same displacements at R_m (Appendix 2). After neglecting higher terms, this gives the equilibrium equation for the pressures needed for solving equation (37)

$$p(r = R_m, t) = \frac{R}{R_m}q(r = R, t) \tag{38}$$

Downloaded by [ETH Zurich] on [12/04/16]. Copyright © ICE Publishing, all rights reserved.

Equations (4), (5), (6), (38) and (35) for $n = 2$ are then substituted into equation (37) and resolved with respect to the constant pressure p_n, which, after being substituted back into pipe deformation equation (35) for $n = 2$, produces for creep conditions ($\sigma_1 = \text{const}$)

$$u^p(\theta, t) = -\frac{2R(1 - K_0)\cos(2\theta)\sigma_1}{E_s + \alpha E_p} \tag{39}$$

where

$$\alpha = \frac{3(5 - \nu_s)I}{R_m^3};\ E_p = \frac{1}{\frac{1}{E_0} + \frac{1}{E_1}(1 - e^{-(E_1/\eta_1)t}) + \frac{1}{\eta_0}t} \tag{40}$$

Next, equations (4), (5), (6), (38) and (36) for $n = 2$ are substituted into equation (37) and resolved with respect to the constant pressure change $\dot{p}_n$, which, after being substituted back into pipe deformation equation (36) for $n = 2$, produces for constant rate conditions ($\dot{\sigma}_1 = \text{const}$)

$$u^p(\theta, t) = -\frac{2R(1 - K_0)\cos(2\theta)\dot{\sigma}_1 t}{E_s + \alpha E_p} \tag{41}$$

where

$$\alpha = \frac{3(5 - \nu_s)I}{R_m^3};$$
$$E_p = \frac{t}{\frac{\eta_1}{E_1^2}(e^{-(E_1/\eta_1)t} - 1) + \frac{1}{2\eta_0}t^2 + \left(\frac{1}{E_0} + \frac{1}{E_1}\right)t} \tag{42}$$

Equations (39) and (41) can be used for interpretation of the IDM measurements by adopting the definition of ovalisation increment from equation (2). Indeed, if the zero measurement is taken before the onset of loading, the major principal lateral pressure increment depends on the measured change in ovalisation value by way of

$$\Delta\sigma_1(t_n) = \frac{E_s + \alpha E_p(t_n)}{8(1 - K_0)\cos(2\beta)}\Delta\Omega(t_n) \tag{43}$$

where t_n is the time of the current measurement, with the time origin taken at the onset of loading; E_p and α are given by equations (40) and (42), for creep and constant rate conditions, respectively; β is the angle between the direction of the inclinometer pipe channels and the direction of principal stresses (Fig. 2).

In case the onset of loading takes place before the zero measurement, equation (43) evolves into the following two equations. For creep conditions, the pressure increment is obtained from the change in ovalisation value measured over the time period (t_0, t_n):

$$\Delta\sigma_1(t_0, t_n) = \frac{\Delta\Omega(t_0, t_n)}{8(1 - K_0)\cos(2\beta)}\frac{1}{\frac{1}{E_s + \alpha E_p(t_n)} - \frac{1}{E_s + \alpha E_p(t_0)}} \tag{44}$$

where E_p and α are given by equation (40) with the time of the zero measurement t_0 and the time of the current measurement t_n measured from the onset of loading.

For constant rate conditions, the pressure increment is given by

$$\Delta\sigma_1(t_0, t_n) = \frac{\Delta\Omega(t_0, t_n)}{8(1 - K_0)\cos(2\beta)}\frac{t_n - t_0}{\frac{t_n}{E_s + \alpha E_p(t_n)} - \frac{t_0}{E_s + \alpha E_p(t_0)}} \tag{45}$$

where E_p and α are defined from equation (42).

The second principal lateral pressure increment is then given by

$$\Delta\sigma_2 = K_0\Delta\sigma_1 \tag{46}$$

Equations (43)–(46) represent analytical formulas allowing for back-calculation of the principal stress increments from the measured ovalisation values of the inclinometer pipe cross-section.

VALIDATION OF THE ANALYTICAL SOLUTIONS

Validation of the solution for the pipe

The analytical solution derived above for the pipe can be validated against laboratory tests on pipe samples performed in a simple test set-up (Fig. 7) by applying two equivalent opposing forces to the pipe in the transversal direction (Schwager *et al.*, 2012).

Loading by two opposite forces $P(t)$ acting at $\theta = 0$ and $\theta = \pi$ can be presented by way of Fourier series

$$p(\theta, t) = -\frac{P(t)}{\pi R_m} - \frac{2P(t)}{\pi R_m}\sum_{n=1}^{n=\infty}\cos(2n\theta) \tag{47}$$

where the first term (hydrostatic pressure) is neglected due to its minor influence on the deformations. After substitution of equation (47) into equations (35) and (36), the solution is given by

$$u(\theta, t) = -\frac{2PR_m^3}{\pi I}\left[\frac{1}{E_0} + \frac{1}{E_1}(1 - e^{-(E_1/\eta_1)t}) + \frac{1}{\eta_0}t\right] \times \sum_{n=1}^{n=\infty}\frac{\cos(2n\theta)}{[(2n)^2 - 1]^2} \tag{48}$$

for creep conditions with constant force P, and

$$u(\theta, t) = -\frac{2\dot{P}R_m^3}{\pi I}\left[\frac{\eta_1}{E_1^2}(e^{-(E_1/\eta_1)t} - 1) + \frac{1}{2\eta_0}t^2 + \left(\frac{1}{E_0} + \frac{1}{E_1}\right)t\right] \times \sum_{n=1}^{n=\infty}\frac{\cos(2n\theta)}{[(2n)^2 - 1]^2} \tag{49}$$

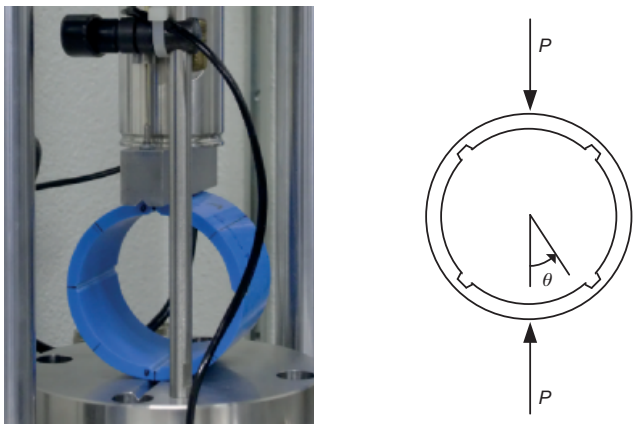


Fig. 7. Laboratory tests performed on pipe samples: (a) test set-up; (b) schematic layout of the test set-up

Downloaded by [ETH Zurich] on [12/04/16]. Copyright © ICE Publishing, all rights reserved.

for constant rate conditions with constant change in force $\dot{P}$.

The inclinometer pipes installed in the landslide areas are assumed to have the same properties as the material of pipe A tested and described in Schwager *et al.* (2012). Parameters of the Burgers model were obtained in independent laboratory tests with pipe compressed in the longitudinal direction. In order to model the transversal behaviour, the stiffness anisotropy in the transversal direction has to be taken into account. This was achieved by reducing the elastic components of the Burgers model by a factor determined from back-analysis of transversal creep tests. This factor was found to be constant for different pipes. Resulting parameters for transversal modelling are presented in Table 1.

The analytical solutions, equations (48) and (49), were validated against results of lab tests, where a sample of the pipe was loaded in the transversal direction by two opposite forces, in both the creep and constant rate modes (Fig. 7(b)). In order to assess the effect of the inclinometer wheel channels, tests were performed on pipe samples at different axes rotation angles and finite-element analysis was used for test interpretation. These tests allowed for successful validation of the viscoelastic model for the true geometry of the channels. Because at the rotation of 45° stiffness reduction caused by the channels is very small, behaviour of the pipe is well described by the analytical solution, allowing for back-calculation of the parameters of the viscoelastic model.

The measured pipe deformations are compared with the analytical solutions provided by equations (48) and (49) using parameters in Table 1 (Fig. 8). Fig. 8(a) shows the comparison between measured and calculated deformations for a creep test lasting 10 days. Fig. 8(b) shows deformations (normalised by the load rate) for four different tests at four different loading rates within four orders of magnitude. The longest test duration is 4 days. As can be seen, both analytical solutions provide remarkably good visual fit to the experimental data and their finite-element simulations.

For other types of the inclinometer casing, parameters of the Burgers model can be found from the longitudinal and transversal compression, creep and constant rate lab tests similar to those presented in Figs 7 and 8.

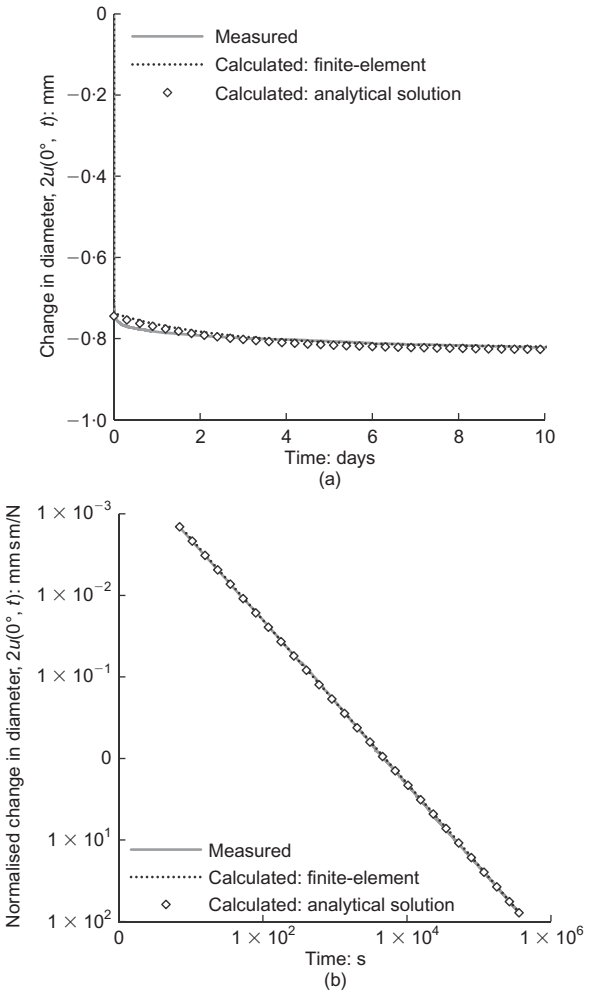


Fig. 8. Comparison of measured and calculated deformations: (a) pipe sample loaded with constant opposite forces of $P = 3636$ N/m; (b) pipe sample loaded in four different tests with constantly increasing opposite forces at the rates of $\dot{P} = 0{\cdot}01$ N/m per s, $\dot{P} = 0{\cdot}1$ N/m per s, $\dot{P} = 1$ N/m per s and $\dot{P} = 10$ N/m per s

Validation of the combined solution

Validation of the combined solution was carried out against the results of numerical simulations, which in turn were validated against results of the full-scale laboratory tests performed in a 200 cm tall calibration chamber with a horizontal cross-section of 40 cm by 40 cm (Figs 9(a) and 9(b)). This two-step procedure allowed for eliminating the effect of the boundaries present in the experimental set-up.

In the first step, a numerical finite-element solution for a 40 cm by 40 cm model was calibrated against laboratory tests (Schwager *et al.*, 2010), where the lateral pressure σ_1 was applied using pressure membranes with constrained kinematic boundary conditions in the perpendicular direction (Fig. 9(b)). At each loading step the soil was assumed linear elastic with its parameters obtained in laboratory tests ($E_s = 9$MPa in initial loading; $E_s = 40$MPa in unloading–reloading; $E_s = 5{\cdot}8$MPa in long-term loading at lower stress level, $\nu_s = 0{\cdot}24$). The viscoelastic four-parameter Burgers model with parameters from Table 1 (Schwager *et al.*, 2012) was used for the material of the pipe, which was modelled using true geometry with channels. As can be seen from Fig. 9, both for the short-term and long-term loading, the finite-element model managed to reproduce the experimental behaviour reasonably well.

Table 1. Parameters of the four-parameter Burgers model for transversal loading of the pipe

Parameter	Value
E_0	2200 MPa
η_0	$3{\cdot}0 \times 10^6$ MPa × day
E_1	21120 MPa
η_1	$5{\cdot}0 \times 10^4$ MPa × day

In the second step, the same numerical model, as validated in the first step, was applied to a different set of boundary conditions, which were closer to those of the analytical solution and more appropriate for the landslide applications. In particular, in order to eliminate effects of the boundaries, dimensions of the horizontal cross-section were increased to 2 m by 2 m. Plane stress conditions were introduced in the vertical direction. The major principal stress, increasing at a constant rate, was applied to one set of the boundaries. On the second perpendicular set of the boundaries, displacements were kinematically constrained. Comparison between numerical and analytical solutions is shown in Fig. 10, where the obtained change in ovalisation value is normalised by the stress rate in kilopascals per year. Although the channels lower the moment of inertia locally, the analytical solution, equations (43)–(46), can provide a good approximation to the numerical one for a broad range of different Young's moduli of soil E_s and different angles β

Downloaded by [ETH Zurich] on [12/04/16]. Copyright © ICE Publishing, all rights reserved.

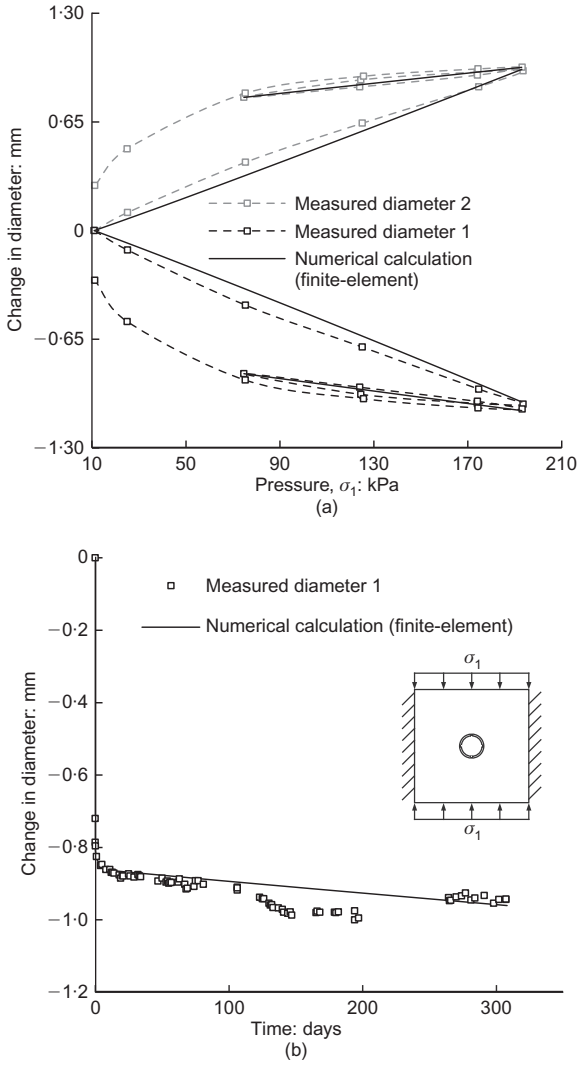


Fig. 9. Change in diameter measured in full-scale laboratory tests and calculated with the finite-element code Abaqus for a 40 × 40 cm model: (a) short-term loading measuring both diameters; (b) long-term loading at constant creep stress ($\sigma_1 = 125$ kPa), measuring only the smaller diameter 1

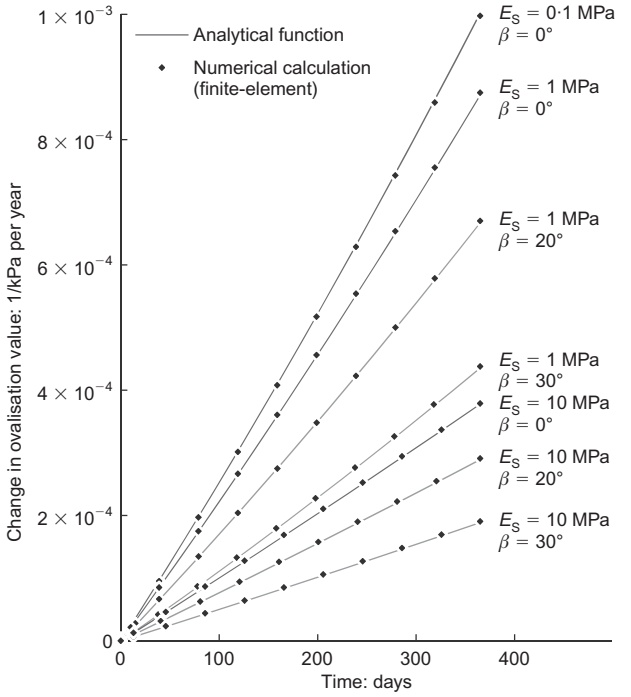


Fig. 10. Change in ovalisation value at constant stress rate: comparison of the analytical solution with finite-element calculations (pipe 84) for a 2 × 2 m model

between the principal stresses and pipe channels (Fig. 10), provided the real thickness of the pipe is reduced to an equivalent value h_{red} (see Table 2).

Table 2. Geometric parameters of the two most common inclinometer pipes used in Switzerland

Symbol	Parameter description	Pipe 84	Pipe 71
R	Outer radius of the pipe	42 mm	35·35 mm
R_m	Mean radius of the pipe	38·925 mm	32·275 mm
h_{red}	Reduced thickness	5·5 mm	5·25 mm

APPLICATION OF THE ANALYTICAL SOLUTIONS TO BACK-CALCULATION OF EARTH PRESSURES IN THE CREEPING LANDSLIDES

Application of the analytical solutions, equations (43)–(46), to back-calculation of increments of earth pressures in creeping landslides requires the knowledge of the soil stiffness and of the principal stresses at the time of the inclinometer pipe installation. These values introduce significant uncertainty into the proposed method, and the present section describes procedures allowing for these uncertainties to be significantly reduced in the back-calculation of the earth pressure increments.

Incorporating in-situ strain measurements

The incremental soil stiffness can be defined from laboratory or field tests, but considering its stress dependency, in particular when the soil exhibits yielding, this requires the knowledge of the in-situ stress state, which is another source of uncertainty. A practical way to reduce these uncertainties is by measuring soil displacements in the vicinity of the inclinometer pipe and calculating the average lateral strain increments $\Delta\varepsilon$. The major principal stress increment $\Delta\sigma_1$ is then expected to occur in the direction of the observed major strain increment (assumed to coincide with the direction of the incremental displacement vector)

$$\Delta\sigma_1(t_0, t_n) = \frac{E_s}{1 - \nu_s^2}\Delta\varepsilon(t_0, t_n) \tag{50}$$

Each of the equations (43)–(45) has two unknowns: the pressure increment and the soil stiffness. Equation (50) has the same two unknowns and, being solved together with one of the equations (43)–(45), appropriate for a particular case under study, would allow for back-calculation of both the principal stress increments and the tangent stiffness of the soil by way of measured ovalisation and average lateral strain.

Assumption of the isotropic initial stress state

Initial stress state after installation of the inclinometer pipe causes creep of the pipe and effects its deformations as described by equations (39) and (40), even if no further changes in the earth pressures take place. When the major principal stress does experience changes (at the constant rate), pipe deformations are described by superposition of solutions (39) and (41). Either way, the solution requires the

Downloaded by [ETH Zurich] on [12/04/16]. Copyright © ICE Publishing, all rights reserved.

knowledge of both principal stresses at the time of installation, which is a source of uncertainty.

This uncertainty can be significantly reduced by using the fact that the drilling of the borehole, installation and grouting of the pipe change the initial stress state around the pipe from anisotropic towards the isotropic state. The isotropic stress state does not contribute to the pipe ovalisation, therefore the creep component of the pipe ovalisation can be neglected, and the only solution to be used for calculating pipe deformations is given by equations (41) and (42), resulting in equation (45), which allows for back-calculation of the major principal stress increment at any point in time, with the time origin taken at the moment of the completion of the pipe installation. The stiffness of PVC in short-term loading is found to be less than 2% higher at 8° compared to 20° (Domininghaus *et al.*, 2008). Therefore, the influence of the temperature difference between the lab and the field on the viscoelastic model seems to be relatively small compared to other uncertainties of the presented approach.

The system of equations (45) and (50) produces a quadratic equation for the soil stiffness, which has only one positive root. This solution is used in analysis of the three case studies presented in the following sections.

CASE STUDY: ST MORITZ-BRATTAS LANDSLIDE, SWITZERLAND

Description

The St Moritz slide is 1500 m long, 600–800 m wide and with average inclination of about 20° (Schlüchter, 1988). This landslide is constrained by the rock outcrop at the bottom of the sliding layer along the Via Maistra (Fig. 11), which can be clearly identified from the contours of yearly horizontal displacements. The displacement rates increase uphill from the rock outcrop, while the field pressures in the sliding layer are expected to increase towards the toe of the slope.

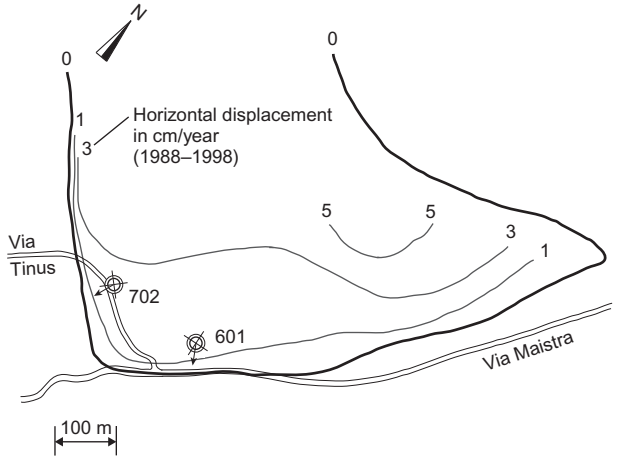


Fig. 11. The St Moritz-Brattas slide with displacement rates and location of the boreholes (after Schlüchter, 1988)

A one-dimensional mechanical model considering the propagation of a zone of intense shearing along the slip surface was proposed for the St Moritz landslide by Puzrin & Schmid (2011). For validation of the model IDM measurements (inclinometer pipe 601) were taken close to the bottom boundary of the landslide (Fig. 11). Additional IDM measurements (inclinometer pipe 702) were performed further away from the bottom boundary, but closer to the side boundary of the landslide.

Long-term stability of the landslide is of the greatest concern for the St Moritz community. Information about the earth pressure changes is essential, because the high pressures in the compression zone are suspected to be the cause of the landslide accelerations.

IDM pressure measurements

IDM measurements were taken in the borehole 601 from 2008 to 2012 (Fig. 11). Inclinometer measurements could be performed in the same borehole from 2008 to 2011, after which the inclinometer probe could not pass through the shear zone any longer. The shear zone is observed at the depth of 16·5 m being less than 0·5 m thick. The average annual displacement at the ground surface is 22 mm. The average annual strain increment $\Delta\varepsilon$ is obtained between the borehole and the landslide boundary of zero displacement (Table 3).

The major principal stress increments are expected to occur in the direction of the observed compressive strain increments, that is, downslope. The change in ovalisation of the pipe measured by IDM confirms the increase in pressures over almost the whole depth and measuring period (Fig. 12). The inner diameter of the pipe in the direction of the slope became smaller with respect to the perpendicular diameter. Hence the ovalisation value is increasing with time. The averaged change of the ovalisation value $\Delta\Omega$ in time is calculated as 0·014%/year for the inclinometer pipe elements between 7·0 m and 12·1 m (the elements close to the ground surface or influenced by the shear zone were not considered).

The corresponding pressure increments and the tangent stiffness of soil can be back-calculated from equations (45) and (50), after substituting equation (42), and accounting for the angle β between the pipe axes and the principal stress directions (Table 3).

The pressure increment $\Delta\sigma_1$ of 0·2 kPa/year compares well with the range of 0·11–1·1 kPa/year for the years 2008–2010 predicted by the analytical model (Puzrin & Schmid, 2011), which concluded that the earth pressure at the bottom reached the passive pressure around 1993.

Table 3. Back-calculation of pressures in the St Moritz slide: parameters of each inclinometer pipe

Parameter description	601	702	Derivation
Year of completion	2006	1990	
Displacement rate	22 mm/year	33 mm/year	Measured
Distance to the boundary	40 m	56 m	Measured
Strain increment, $\Delta\varepsilon$	0·056%/year	0·059%/year	Measured
Change in ovalisation value, $\Delta\Omega$	0·014%/year	0·088%/year	Measured
Angle of the pipe, β	22·2°	19·3°	Measured
Deformation modulus of the soil, E_s	0·3 MPa	0·6 MPa	Back-calculated
Pressure increment, $\Delta\sigma_1$	0·2 kPa/year	0·4 kPa/year	Back-calculated

Downloaded by [ETH Zurich] on [12/04/16]. Copyright © ICE Publishing, all rights reserved.

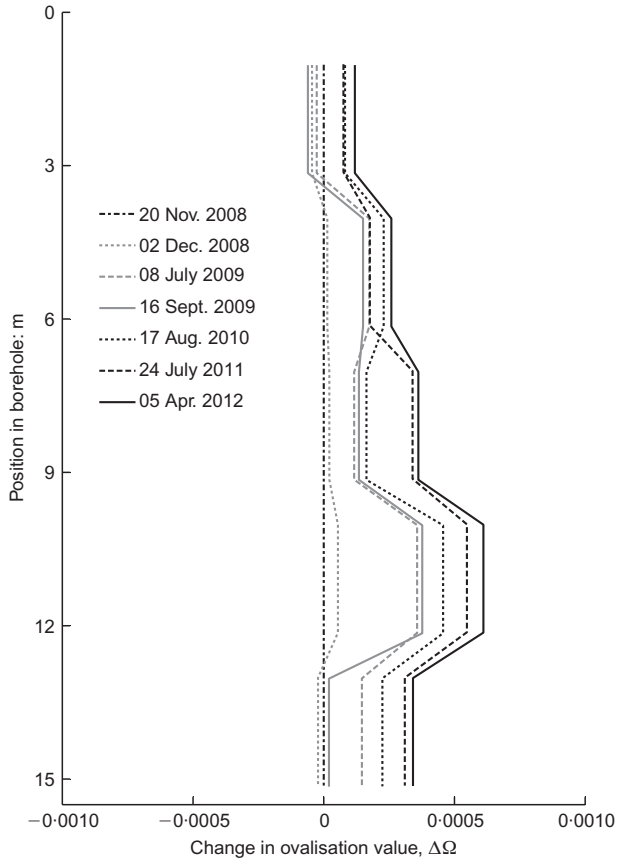


Fig. 12. Pipe deformation of inclinometer 601 measured by IDM, St Moritz

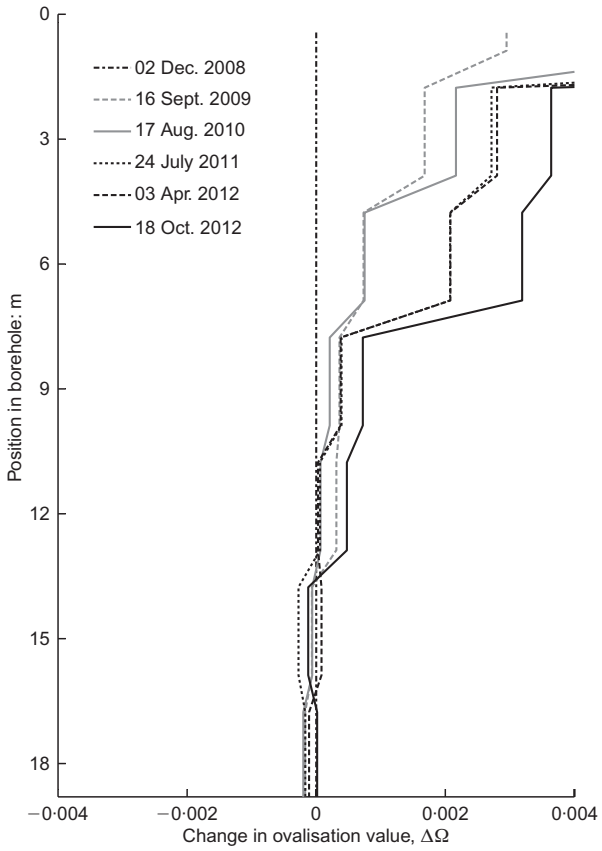


Fig. 13. Pipe deformation of inclinometer 702 measured by IDM, St Moritz

Comparing the very small back-calculated deformation modulus of the soil E_s of 0·3 MPa with the elastic modulus of 17·9 MPa based on Marchetti dilatometer tests (Puzrin *et al.*, 2008; Puzrin & Schmid, 2011) confirms that the soil exhibits secondary compression and post-failure hardening.

IDM measurements were also taken in borehole 702 (Fig. 11) in the inclinometer pipe, which was sheared in 1997. The location of the slip surface at a depth of 21 m and the direction of the displacement vector are known from inclinometer measurements performed from 1995 to 1997. The current displacement rate of 33 mm/year is obtained from nearby geodetic measurements. Although the strain rate is similar to that of inclinometer 601, the change in ovalisation value $\Delta\Omega$ is considerably higher in the upper part of the borehole (Fig. 13 and Table 3). Pipe elements from 1·8 m to 6·8 m were taken for averaging. In spite of the larger change in ovalisation, the back-calculated deformation modulus E_s of 0·6 MPa and the pressure increment of 0·4 kPa/year are comparable to those in the borehole 601. This again confirms the soil failure, strain hardening and secondary compression in the compression zone, while the larger change in ovalisation in the pipe of the borehole 702 can be explained by the fact that it was installed 16 years earlier than the pipe in the borehole 601, resulting in the lower viscoelastic stiffness of the pipe.

CASE STUDY: BRAUNWALD LANDSLIDE, SWITZERLAND

Description

The village of Braunwald (Fig. 14) is built on a natural terrace with an area of 4 km^2, creeping towards the cliff facing the valley (Schindler, 1982; Schindler & Rageth, 1990), resulting at the bottom in an active pressure boundary condition.The slip surface is inclined by only 10–12° and mostly formed within a several-metres-thick clay layer of weathered schist above the moraine (Fig. 15).

The upper part of the terrace is moving as one block, while the sliding mass in the lower part of the landslide is moving faster towards the cliffs (Fig. 16). Locally, high spontaneous acceleration can be observed in the area close to the cliffs. Smaller local slides of several 10 000 m^3 are often triggered by heavy rainfall and fall over the cliffs. The authorities expect such larger events to happen every 15–20 years. Some parts of the village are located close to the cliffs.

The observed gradient in the displacement rate suggests that earth pressures in the sliding layer are expected to decrease towards the boundary. IDM measurements were performed in two boreholes (inclinometers KB2 and KB6) in the lower part of the landslide, where most of the buildings and infrastructure are located.

IDM pressure measurements

Borehole KB2 is located next to the cable car station in an area of larger movements close to the cliff (Fig. 16). The inclinometer pipe in the borehole has been sheared at the slip surface 10·5 m below the ground surface before 2009. The current ground movement of 34 mm/year is known from a permanent global positioning system (GPS) station installed at the station of the cable car. The strain rate of −0·034%/year has been derived between KB2 and a nearby inclinometer located in the same slope profile for the period of 2002–2006.

Borehole KB6 is located in a different area further up the slope, where the observed displacements are smaller (Fig. 16). The inclinometer pipe has not yet been sheared.

Downloaded by [ETH Zurich] on [12/04/16]. Copyright © ICE Publishing, all rights reserved.

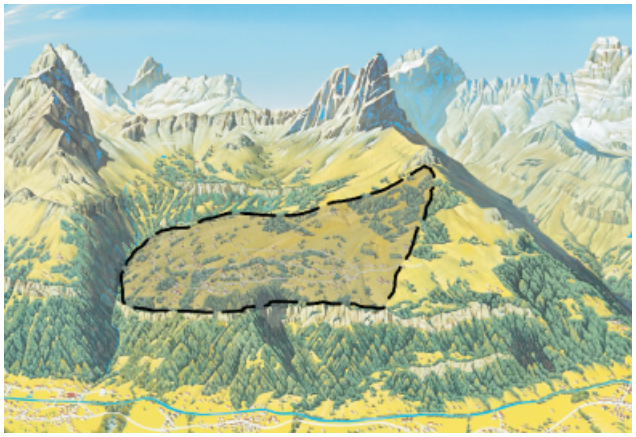


Fig. 14. The sliding terrace of Braunwald (after Braunwald-Klausenpass Tourismus)

Nevertheless, IDM measurements have only been possible in the top 27 m. Inclinometer measurements show a surface displacement of 8 mm/year. The strain rate of −0·011%/year for the period of 2009–2012 is obtained by considering another inclinometer further downhill in the same profile. Constant gradient in the displacement rate is assumed over the distance between the inclinometers.

IDM measurements were performed in both inclinometer pipes in the period between 2009 and 2012 (Figs 17 and 18). The pipe elements in KB6 above the depth of 13·4 m were ignored, owing to possible local shallow slides in the area. Negative change in ovalisation value $\Delta\Omega$ clearly indicates extension in the slope direction. The pipe diameter in the direction of the slope becomes larger with time with respect to the perpendicular diameter. The observed changes in ovalisation value $\Delta\Omega$ are similar in both boreholes (Table 4), whereas the strain rates are different. The pressure increments and the deformation moduli of the soil are back-calculated solving the set of equations (45) and (50), showing, as expected, a lower tangent stiffness and pressure drop at KB2, closer to the cliff where the soil has failed in the active mode (Table 4). Away from the cliff, at KB6, the soil experiences less yielding, but a very low back-calculated soil stiffness indicates its possible rate dependency.

CASE STUDY: GANTER LANDSLIDE, SWITZERLAND

Description

The Simplon Pass connects Switzerland to Italy by way of the Alps. In 1980 a bridge was built crossing the valley 140 m over the Ganter river (Menn, 1979). On the left bank of the river, the bridge is founded on a creeping landslide. The slope is inclined by 24° and covers an area of about 0·4 km^2. The ground surface next to the new bridge is moving at a rather uniform velocity of 4·2 mm/year, as measured in the period from 1994 to 2004 (Puzrin & Schmid, 2012). Inclinometer measurements show displacements decreasing almost linearly with depth within the sliding body (Ritz, 1992). The soil consists of slope debris, moraine and stones of schist (Schaerer, 1975).

The landslide is creeping towards the Ganter river and is constrained by the rock outcrop at the opposite riverbank. Puzrin & Schmid (2012) have concluded that the soil close to the riverbed has reached passive failure. IDM measurements were performed in two boreholes (inclinometer 702 and 704) next to the river in the zone where the soil has possibly failed (Fig. 19).

IDM pressure measurements

Boreholes 702 and 704 are located at a distance of 17 m and 28 m from the opposite river bank, respectively. IDM and inclinometer readings were taken in the period from 2010 to 2012. The displacement rate at the surface is observed to be 1·1 mm/year in the borehole 702. The displacements are decreasing with depth; no clear shear surface could be identified.

An averaged strain rate of 0·006%/year is obtained both between borehole 702 and the boundary and between 702 and the closest uphill geodetical measurement point (Table 5). For the borehole 704, the strain rate is assumed to be the same. In both boreholes, the change in ovalisation value $\Delta\Omega$ is observed to be very small averaged over the depth of the boreholes (Fig. 20 and Fig. 21). The measured absolute deformations of the pipe of 0·5 μm for the period are within the precision of the IDM device of ±2 μm. Therefore in practice the change in ovalisation value $\Delta\Omega$ can be considered to be very close to zero, resulting from equations (45) and (50) in zero values of both the pressure increment $\Delta\sigma_1$ and the deformation modulus of the soil E_s, confirming the passive failure of the soil close to the bottom boundary of the landslide (for details see Puzrin & Schmid, 2012).

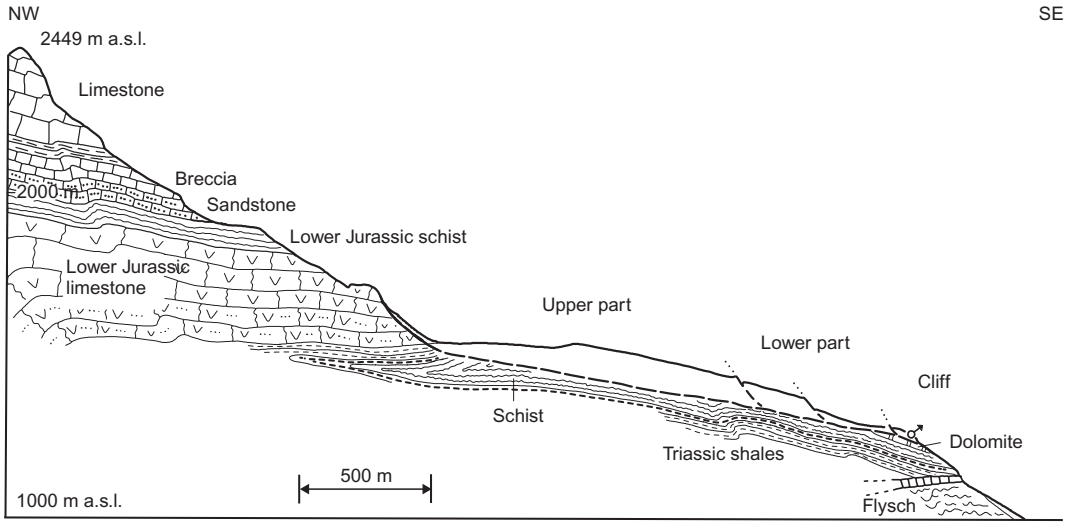


Fig. 15. The geology of the Braunwald slide (after Schindler, 1982)

Downloaded by [ETH Zurich] on [12/04/16]. Copyright © ICE Publishing, all rights reserved.

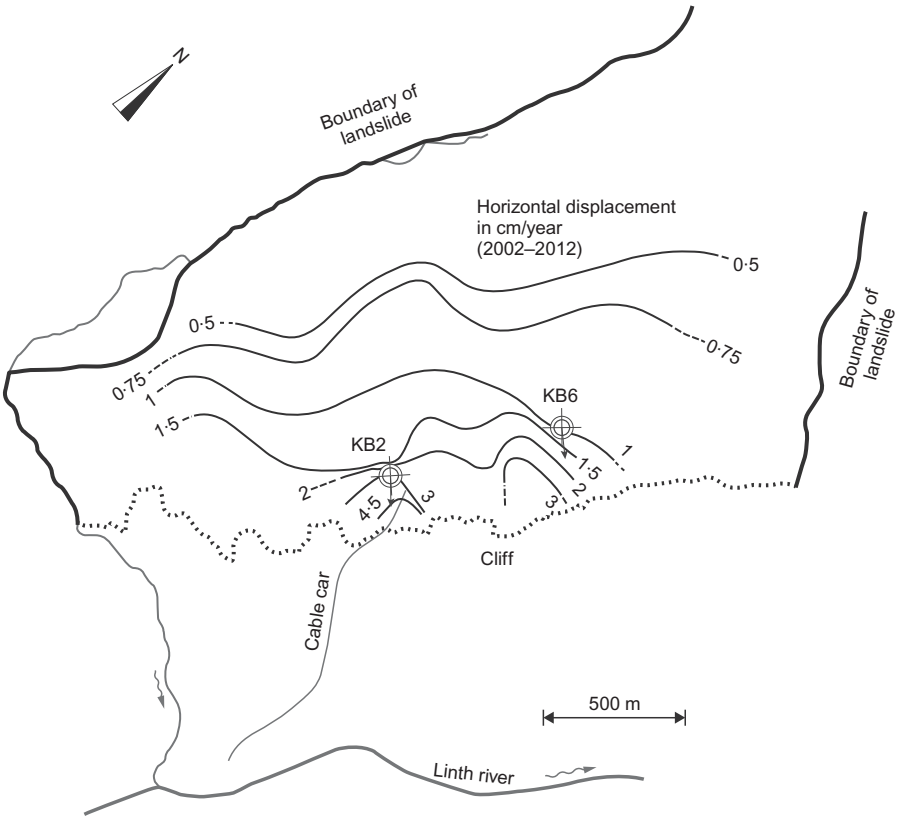


Fig. 16. The Braunwald slide with displacement rates and location of the boreholes

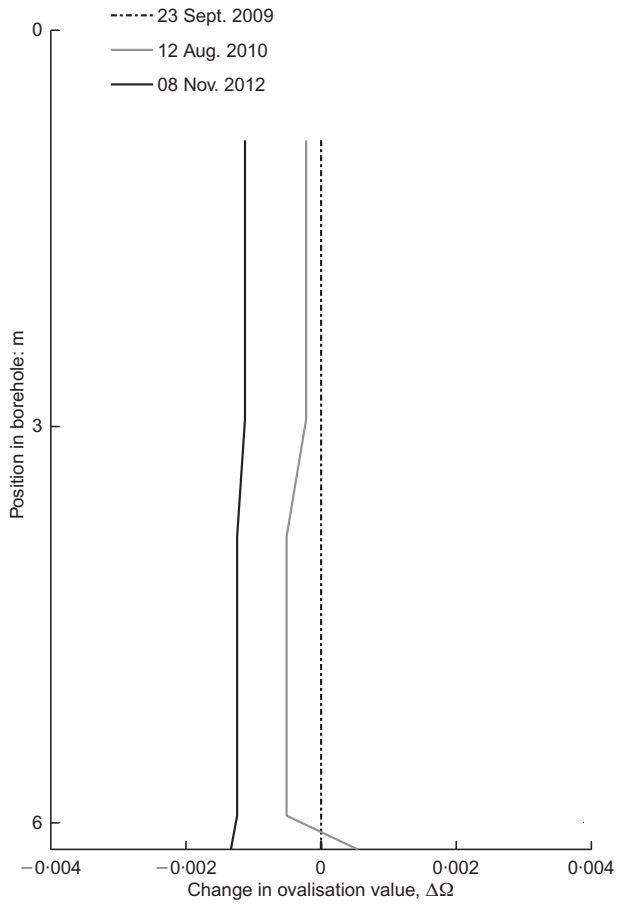


Fig. 17. Pipe deformation of inclinometer KB2 measured by IDM, Braunwald

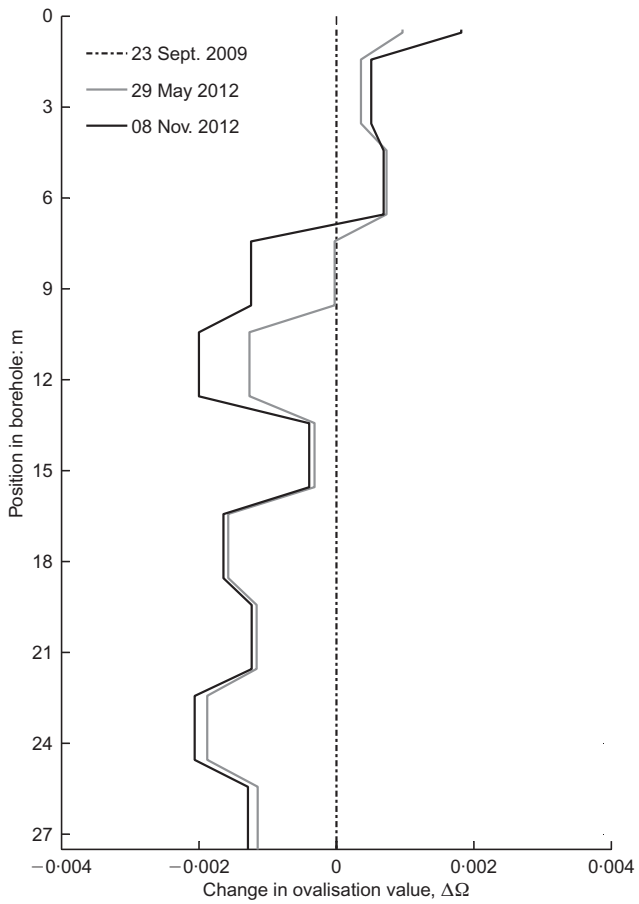


Fig. 18. Pipe deformation of inclinometer KB6 measured by IDM, Braunwald

Downloaded by [ETH Zurich] on [12/04/16]. Copyright © ICE Publishing, all rights reserved.

Table 4. Back-calculation of pressures in the Braunwald slide: parameters of each inclinometer pipe

Parameter description	KB2	KB6	Derivation
Year of completion	2002	2002	
Displacement rate	34 mm/year	8 mm/year	Measured
Distance to the cliff	180 m	360 m	Measured
Strain increment, $\Delta\varepsilon$	−0·034%/year	−0·011%/year	Measured
Change in ovalisation value, $\Delta\Omega$	−0·038%/year	−0·042%/year	Measured
Angle of the pipe, β	2·4°	5·6°	Measured
Deformation modulus of the soil, E_s	0·6 MPa	4·3 MPa	Back-calculated
Pressure increment, $\Delta\sigma_1$	−0·2 kPa/year	−0·5 kPa/year	Back-calculated

SUMMARY AND CONCLUSIONS

The paper derives analytical solutions for deformation of viscoelastic pipe in elastic soil under far-field principal stress increments. These solutions are validated in laboratory tests and numerical analysis and provide the basis for back-calculation of earth pressure increments from measured changes in shape of an inclinometer pipe cross-section using IDM technology. The procedure has then been applied to back-calculating earth pressure changes in three creeping landslides in Switzerland, which are similar in size but have a range of different boundary conditions and displacement rate fields

(*a*) the St Moritz-Brattas landslide, which is slowing downhill towards a rock outcrop at the bottom
(*b*) the Braunwald landslide, which is accelerating downhill towards a vertical rock wall falling into a valley
(*c*) the Ganter landslide, which is moving uniformly downhill towards a river bed.

In these applications, reasonably small pressure increments could be reliably back-calculated by applying the obtained analytical solution which takes the time-dependency of the pipe material properties into account. These pressure increments allowed for identification of compression and extension zones in the landslides under study, confirming the previously developed models of the landslide mechanisms.

Combining the IDM measurements with measurements of relative displacements, the tangent stiffness of the soil could also be clearly identified. The obtained in-situ deformation modulus for the incremental behaviour indicates yielding, failure and possibly secondary compression of soil, confirming the previous landslide analysis and suggesting that IDM pressure measurements could serve as a reliable tool for analysis and monitoring of creeping landslides.

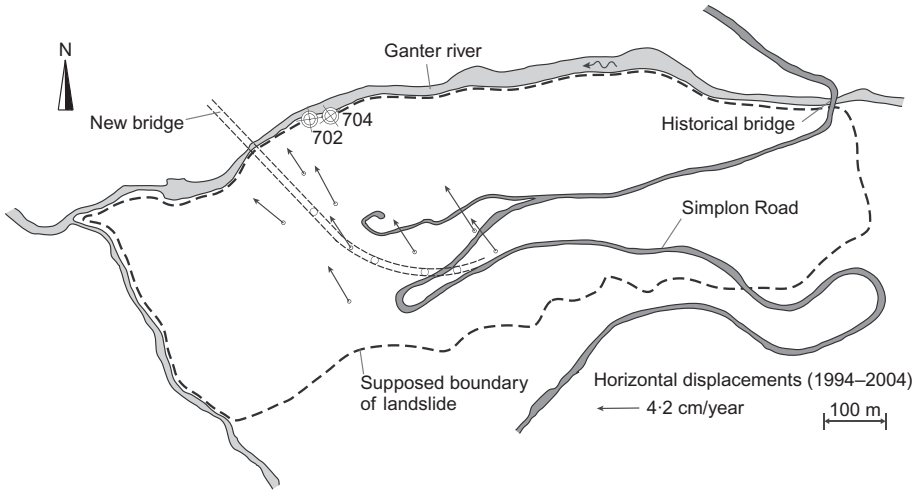


Fig. 19. The Ganter slide with displacement rates and location of the boreholes

Table 5. Back-calculation of pressures in the Ganter slide: parameters of each inclinometer pipe

Parameter description	702	704	Derivation
Year of completion	2007	2007	
Displacement rate	1·1 mm/year	–	Measured
Distance to the boundary	17 m	28 m	Measured
Strain increment, $\Delta\varepsilon$	0·006%/year	0·006%/year	Measured
Change in ovalisation value, $\Delta\Omega$	−0·0007%/year	−0·0007%/year	Measured
Angle of the pipe, β	13·8°	–	Measured
Deformation modulus of the soil, E_s	Small	Small	Back-calculated
Pressure increment: $\Delta\sigma_1$	Small	Small	Back-calculated

Downloaded by [ETH Zurich] on [12/04/16]. Copyright © ICE Publishing, all rights reserved.

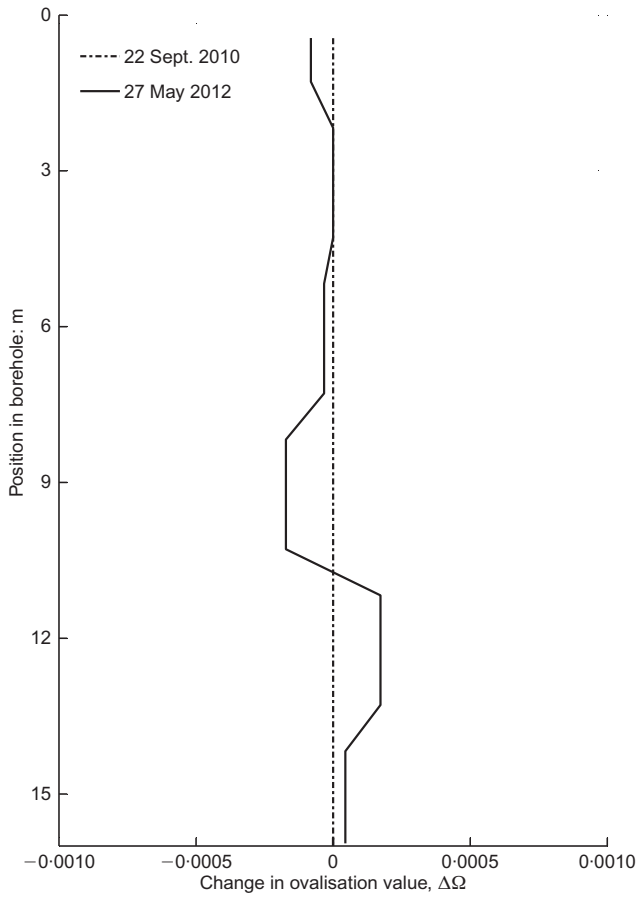


Fig. 20. Pipe deformation of inclinometer 702 measured by IDM, Ganter

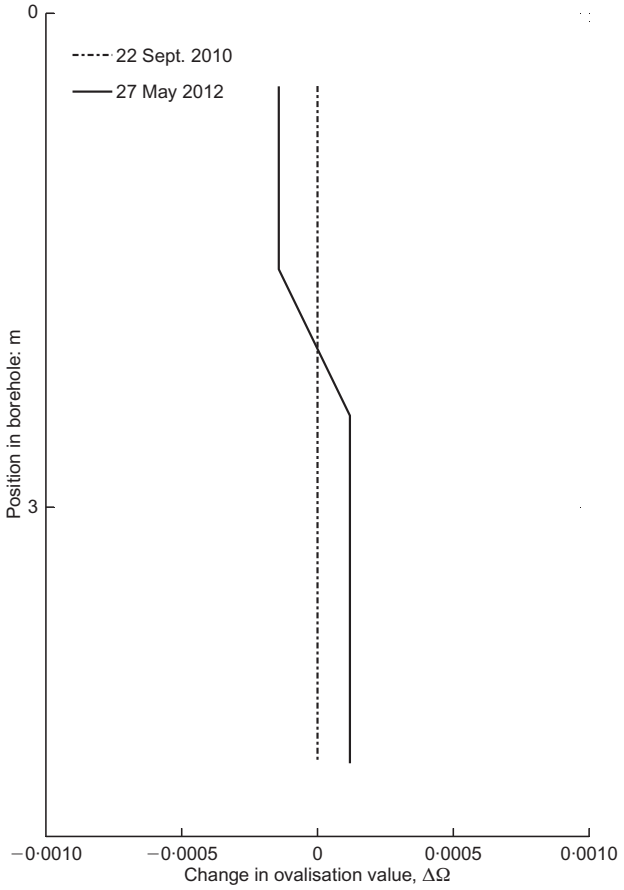


Fig. 21. Pipe deformation of inclinometer 704 measured by IDM, Ganter

ACKNOWLEDGEMENTS

The contributions of F. Fischli, P. Oberender, A. Schmid and S. Zweidler, all of the ETH Zurich, to this study are highly appreciated. The authors would like to thank the authorities of St Moritz and Braunwald and the Department of Construction of Canton du Valais for providing data on the displacements of the landslides. The work has been partially supported by the ASTRA/VSS (grant no. VSS 2010/502) 'Landslide-Road-Interaction: Applications'.

APPENDIX 1: VISCOELASTIC CONSTITUTIVE EQUATIONS IN TERMS OF PIPE FORCES

Derivation of the constitutive relationships for a thin pipe in terms of its forces and moments uses compatibility considerations (Bouma, 1993) to obtain the strain distribution across the thickness of the pipe (Fig. 5(b))

$$\varepsilon(z) = \frac{R_m}{R_m + z}(\varepsilon_0 + \chi z) \tag{51}$$

The normal force and the moment are defined as

$$N = \int_{-h/2}^{h/2} \sigma(z)\mathrm{d}z \tag{52}$$

$$M = \int_{-h/2}^{h/2} \sigma(z) z\,\mathrm{d}z \tag{53}$$

where h is the thickness of the pipe.

The constitutive equation in terms of circumferential stresses and strains follows from the Burgers model

$$\sigma + p_1\dot{\sigma} + p_2\ddot{\sigma} = q_1\dot{\varepsilon} + q_2\ddot{\varepsilon} \tag{54}$$

Integrating both sides of equation (54) and substituting equations (52) and (53) into it gives

$$N + p_1\dot{N} + p_2\ddot{N} = q_1 \int_{-h/2}^{h/2} \dot{\varepsilon}(z)\mathrm{d}z + q_2 \int_{-h/2}^{h/2} \ddot{\varepsilon}(z)\mathrm{d}z \tag{55}$$

$$M + p_1\dot{M} + p_2\ddot{M} = q_1 \int_{-h/2}^{h/2} \dot{\varepsilon}(z)z\mathrm{d}z + q_2 \int_{-h/2}^{h/2} \ddot{\varepsilon}(z)z\mathrm{d}z \tag{56}$$

Next, expressing equation (51) as Taylor series (Bouma, 1993), substituting it into equations (55) and (56), integrating and neglecting terms of higher order than h^4 (thin pipe), results in the following constitutive relationships for a thin pipe in terms of the forces and moments

$$N + p_1\dot{N} + p_2\ddot{N} = q_1\left(A\dot{\varepsilon}_0 - \frac{I}{R_m}\dot{\chi}\right) + q_2\left(A\ddot{\varepsilon}_0 - \frac{I}{R_m}\ddot{\chi}\right) \tag{57}$$

$$M + p_1\dot{M} + p_2\ddot{M} = q_1\left(-\frac{I}{R_m}\dot{\varepsilon}_0 + I\dot{\chi}\right) + q_2\left(-\frac{I}{R_m}\ddot{\varepsilon}_0 - I\ddot{\chi}\right) \tag{58}$$

where $A = 1 \times h$ is the area and $I = 1 \times h^3/12$ is the moment of inertia of the pipe cross-section.

APPENDIX 2: EQUIVALENT PRESSURE ACTING ON A THIN-WALLED PIPE

A thin-walled pipe approximation requires a correspondence principle transforming the pressure q acting at the outer surface of the pipe at $r = R = R_m + h/2$ into the pressure p acting on the thin ring of the median radius $r = R_m$ (Fig. 22). This principle is based

Downloaded by [ETH Zurich] on [12/04/16]. Copyright © ICE Publishing, all rights reserved.

on the condition that pressures q and p should produce the same radial displacements at the same $r = R_m$ for a thick-walled and a thin-walled pipe, respectively.

First, the thick-walled pipe with thickness h is considered to be under pressure $-q\cos(2\theta)$ at the outer radius $r = R = R_m + h/2$.

The solution for the radial displacement at the centre of the cross-section is given by the Michell solution (Barber, 2002) as

$$u_{thick}(r = R_m, \theta) = -\frac{4R_m^4 q\cos(2\theta)}{3Eh^3} \times \left(1 + \frac{h}{2R_m} + \frac{3h^2}{4R_m^2} + \frac{3h^2\nu}{8R_m^2} + \frac{h^3}{4R_m^3} + \frac{5h^3\nu}{16R_m^3} - \frac{29h^4}{128R_m^4} + \frac{5h^4\nu}{128R_m^4} - \frac{9h^5}{256R_m^5} - \frac{3h^5\nu}{256R_m^5} + \frac{13h^6}{512R_m^6} + \frac{h^6\nu}{512R_m^6} + \frac{5h^7}{512R_m^7} + \frac{h^7\nu}{256R_m^7} + \frac{9h^8}{2048R_m^8} + \frac{3h^8\nu}{2048R_m^8} - \frac{h^9}{4096R_m^9} - \frac{h^9\nu}{4096R_m^9} - \frac{h^{10}}{8192R_m^{10}} - \frac{h^{10}\nu}{8192R_m^{10}}\right) \quad (59)$$

According to the correspondence principle, pressure $-q\cos(2\theta)$, acting at the outer radius $r = R = R_m + h/2$ of the thick-walled pipe, should produce in this pipe at $r = R_m$ the same radial displacements as the pressure $-p\cos(2\theta)$, acting on the equivalent thin pipe of the radius R_m, would produce in the thin pipe

$$u_{thin}(r = R_m, \theta, p) = u_{thick}(r = R_m, \theta, q) \quad (60)$$

The radial displacement of the thin pipe is given by equation (24) for $n = 2$ and $I = h^3/12$ as

$$u_{thin}(r = R_m, \theta) = -\frac{4R_m^4}{3Eh^3} p\cos(2\theta) \quad (61)$$

Substituting equations (59) and (61) into equation (60) and neglecting the higher order terms gives the ratio p/q

$$p(r = R_m)/q(r = R) \approx 1 + \frac{h}{2R_m} = R/R_m \quad (62)$$

which provides the necessary equivalent pressure acting on a thin pipe

$$p(r = R_m) = \frac{R}{R_m} q(r = R) \quad (63)$$

NOTATION

A	cross-sectional area of pipe
D_A	inner diameter of pipe within channels in direction A
$D_{A,0}$	zero measurement of inner diameter of pipe in direction A
$D_{A,n}$	further measurement of inner diameter of pipe in direction A
D_B	inner diameter of pipe within channels in direction B
$D_{B,0}$	zero measurement of inner diameter of pipe in direction B
$D_{B,n}$	further measurement of inner diameter of pipe in direction B
E	Young's modulus of pipe
$\hat{E}$	transformed modulus of pipe
E_g	Young's modulus of grout
E_p	time-dependent pipe stiffness parameter
E_s	Young's modulus of soil
E_0	elastic parameter of Burgers model
E_1	elastic parameter of Burgers model
h	thickness of pipe
h_{red}	reduced thickness of inclinometer pipe
I	moment of inertia of cross-section of pipe
K_0	(incremental) earth pressure coefficient within horizontal plane
M	bending moment in pipe
$\hat{M}$	transformed moment
N	normal force in pipe
$\hat{N}$	transformed normal force
P	force acting on pipe
p	pressure acting on pipe
$\hat{p}$	transformed pressure
p_1	parameter of viscoelastic Burgers model
p_2	parameter of viscoelastic Burgers model
q	pressure acting on cavity
q_1	parameter of viscoelastic Burgers model
q_2	parameter of viscoelastic Burgers model
R	nominal outer radius of inclinometer pipe, radius of cavity
R_m	mean radius of pipe
r	radial coordinate
s	Laplace variable
t	time
t_0	time of zero measurement
t_n	time of current measurement
u	radial displacement
$\hat{u}$	transformed radial displacement
u_{thick}	radial displacement of thick-walled pipe
u_{thin}	radial displacement of equivalent thin-walled pipe
u^p	radial deformation of pipe due to external pressure
u^q	radial deformation of soil due to pressure at inclusion
u^{σ_1}	radial deformation of soil due to lateral earth pressure
V	shear force in pipe
v	tangential displacement
$\hat{v}$	transformed tangential displacement
z	coordinate within cross-section of pipe
α	dimensionless coefficient
α_L	inclination of lever
α_P	inclination of probe
β	angle between pipe channels and direction of principal stresses
$\gamma_{r\theta}$	shear strain
$\Delta\varepsilon$	lateral principal strain increment
$\Delta\sigma_1$	major principal stress increment in horizontal plane
$\Delta\sigma_2$	minor principal stress increment in horizontal plane
$\Delta\Omega$	change in ovalisation value
ε	strain
ε_1	lateral principal strain
ε_0	axial strain in pipe
$\hat{\varepsilon}_0$	transformed axial strain
ε_r	radial strain
ε_θ	tangential strain
η_0	viscous parameter of Burgers model
η_1	viscous parameter of Burgers model
θ	circumferential coordinate
ν_g	Poisson ratio of grout
ν_p	Poisson ratio of pipe
ν_s	Poisson ratio of soil
σ	stress
σ_1	principal stress within horizontal plane
σ_2	principal stress within horizontal plane
σ_r	normal stress in radial direction
σ_θ	normal stress in tangential direction
$\tau_{r\theta}$	shear stress
χ	transversal curvature in pipe wall
$\hat{\chi}$	transformed transversal curvature in pipe wall
χ_0	initial longitudinal curvature of pipe
χ_n	current longitudinal curvature of pipe

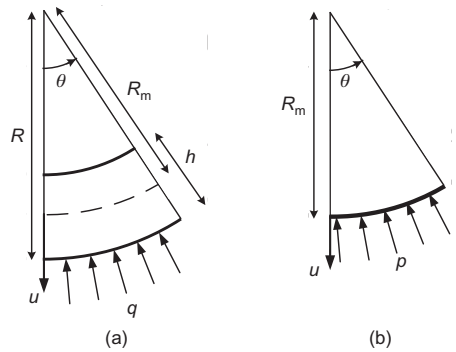


Fig. 22. (a) Pressure q acting on the thick-walled pipe; (b) pressure p acting on the equivalent thin-walled pipe

Downloaded by [ETH Zurich] on [12/04/16]. Copyright © ICE Publishing, all rights reserved.

Ω ovalisation value
Ω_0 zero measurement of ovalisation value
Ω_n further measurement of ovalisation value

REFERENCES

Barber, J. R. (2002). *Elasticity*. Dordrecht, the Netherlands and Boston, MA, USA: Kluwer Academic Publishers.

Bouma, A. L. (1993). *Mechanik schlanker Tragwerke: Ausgewählte Beispiele in der Praxis*. Berlin, Germany: Springer Verlag (in German).

Domininghaus, H., Elsner, P., Eyerer, P. & Hirth, T. (2008). *Kunststoffe, Eigenschaften und Anwendungen*. Berlin, Germany: Springer Verlag (in German).

Findley, W. N., Lai, J. S. & Onaran, K. (1976). *Creep and relaxation of nonlinear viscoelastic materials – with an introduction to linear viscoelasticity*. Amsterdam, the Netherlands: North-Holland Publishing Company.

Menn, C. R. H. (1979). Ganterbrücke. *Schweiz. Ing. Architekt* **97**, No. 38, 733–739 (in German).

Penzien, J. & Wu, C. L. (1998). Stresses in linings of bored tunnels. *Earthquake Engng Struct. Dynamics* **27**, No. 3, 283–300.

Puzrin, A. M. & Schmid, A. (2011). Progressive failure of a constrained creeping landslide. *Proc. R. Soc. A – Math. Phys. Engng Sci*. **467**, No. 2133, 2444–2461.

Puzrin, A. M. & Schmid, A. (2012). Evolution of stabilised creeping landslides. *Géotechnique* **62**, No. 6, 491–501, http://dx.doi.org/10.1680/geot.11.P.041.

Puzrin, A. M., Messerklinger, S. & Schmid, A. (2008). The in-situ stiffness of the sliding layer in a creeping landslide. *Proceedings of the 4th international symposium on deformation characteristics of geomaterials, Atlanta* (eds S. E. Burns, P. W. Mayne and J. C. Santamarina), vol. 1, pp. 407–412. Amsterdam, the Netherlands: IOS Press.

Puzrin, A. M., Schmid, A. & Schwager, M. V. (2012). Case studies of constrained creeping landslides in Switzerland. *Proceedings of the 11th international symposium on landslides and engineered slopes ISL, Banff, Canada* (eds E. Eberhardt, C. Froese, A. K. Truner and S. Leroueil), vol. 2, pp. 1795–1800. Leiden, the Netherlands: CRC Press/Balkema.

Ritz, P. (1992). Überwachung der Ganterbrücke. *Strasse Verkehr* **78**, No. 5, 345–349 (in German).

Schaerer, C. (1975). Ueberquerung des Ganterbaches. *Mitteilungen Schweizerischen Gesellschaft Boden Felsmechanik* **91**, Spring, 1–4 (in German).

Schindler, C. (1982). Problemreiche Hinterlassenschaft: Geologie und Wasserverhältnisse in Braunwald. *Neujahrsbote für das Glarner Hinterland (Grosstal und Sernftal), 1982* (ed. H. Stüssi), no. 16, pp. 131–140. Glarus, Switzerland: Spältie & Cie (in German).

Schindler, C. & Rageth, R. (1990). Braunwald (Swiss alps) – investigation, analysis and partial stabilization of a big landslide. *Proceedings of 6th international congress: International Association of Engineering Geology* (ed. D. G. Price), vol. 3, pp. 1705–1711. Rotterdam, the Netherlands: Balkema.

Schlüchter, C. (1988). Instabilities in the area of St. Moritz, Switzerland – Geology, chronology, geotechnology. *Proceedings of the 5th international symposium on landslides, Lausanne* (ed. Ch. Bonnard), vol. 2, pp. 1375–1380. Rotterdam, the Netherlands: Balkema.

Schwager, M. V. (2013). *Development, analysis and applications of an 'inclinodeformeter' device for earth pressure measurements*. Phd thesis, ETH, Zurich, Switzerland.

Schwager, M. V., Schmid, A. M. & Puzrin, A. M. (2010). Inclinodeformometer for earth pressure measurements in creeping landslides. *Soils Found*. **50**, No. 4, 451–458.

Schwager, M. V., Oberender, P. W. & Puzrin, A. M. (2012). Effects of time dependency on earth pressure measurements taken by inclinodeformometer. *Proceedings of the 4th international conference on geotechnical and geophysical site characterization, Porto de Galinhas, Brazil* (eds R. Q. Coutinho and P. W. Mayne), pp. 571–577. Boca Raton, FL, USA: CRC Press.

Downloaded by [ETH Zurich] on [12/04/16]. Copyright © ICE Publishing, all rights reserved.
View publication stats